

Parametric EIT for Monitoring Cardiac Stroke Volume

Zlochiver S., Freimark D. *, Arad M. §, Adunsky A. §, Abboud S.

Tel-Aviv University, Department of Biomedical Engineering

*Department of Cardiology, Sheba Medical Center, Ramat-Gan, Israel

§Department of Geriatric Rehabilitation, Sheba Medical Center, Ramat-Gan, Israel

ABSTRACT: The bio-impedance technique appears appropriate for non-invasive cardiac stroke volume (SV) measurement, as the thoracic conductivity distribution is altered during the cardiac-cycle due to the heart contraction and blood perfusion. In the present work, the feasibility of a parametric EIT for assessing the cardiac SV was studied. An impedance model of the thorax was constructed from segmented axial MRI images along 19 phases of the cardiac-cycle. The heart was simulated as an ellipsoid, with its axes' lengths set as the reconstruction parameters, while all other tissues' geometry and conductivity values were kept fixed. A Newton-Raphson parametric optimization scheme was utilized, yielding a correlation between the reconstructed and anatomical left ventricular volumes of 0.97 ($p=2 \cdot 10^{-11}$). An analysis of noise sensitivity showed that the proposed algorithm requires an SNR greater than 65dB. The simulation results were compared to physical data, collected with a portable EIT system (PulmoTrace™, CardioInspect). The validation study was employed for a group of N=28 healthy patients, and a comparison with impedance-cardiography measurements (BioZ[®], Cardiodynamics) was performed, showing a correlation of $r=0.86$ ($p=4 \cdot 10^{-9}$). The preliminary results demonstrate that parametric EIT has the potential to measure SV, and may be applicable for both clinical and home-environment usage.

1. INTRODUCTION

As a direct indicator to the global cardiac pumping efficiency, the cardiac Stroke Volume (SV) has major diagnostic value in numerous conditions, including cardiovascular disease, congestive heart failure, hypertension, acute coronary syndromes, coronary artery disease, ischemia and optimization of pacemaker or intra-aortic balloon pump. There are big changes in the thoracic conductivity distribution during the cardiac cycle, due to high-conducting blood perfusion from the heart to the various tissues, mechanical movements of the heart, and dilation of blood vessels. These temporal spatial conductivity changes suggest that the impedance technique may be appropriate for measuring the cardiac related SV. In 1959, a technique called impedance cardiography was introduced⁸, where the stroke volume is calculated from the changes in the transthoracic electrical resistivity. In the most common configuration⁵, four band electrodes are attached to the thorax proximities, from which current is injected and impedance is measured, and the stroke volume is calculated from the recorded signals by considering a parallel column model and assuming that the impedance change is mostly originating from the blood perfusion to the lungs. Though compared and found in good correlation to other SV measuring techniques⁶, no conclusive results were obtained. One of the most problematic issues in this technique is that only global information is retrieved, and the relative contribution of the various thoracic organs to the total impedance during the cardiac cycle is not clear⁹. EIT seems to overcome this limitation by solving for the

spatial conductivity distribution. Several simulation and in-vivo works have studied the feasibility of EIT for imaging cardiac related thoracic impedance changes, usually using generic EIT systems employing either two or three-dimensional models⁷. Still, EIT has major technical limitations, mainly due to the requirement to attach a large number of electrodes to the patient's thorax and its high sensitivity to measurement noise, either electrical or geometrical. EIT is therefore currently employed mostly in research studies, using laboratory systems, and is not practiced in the clinics. In the present work, a parametric EIT algorithm for monitoring SV was developed. The algorithm was primarily intended to perform fast and be less sensitive to measurement noise, making it applicable for clinical system embedment. The algorithm was evaluated both in simulation and in a clinical study using a portable EIT system (PulmoTrace™, CardioInspect, Tel-Aviv University, Israel), which consists of an eight-electrode thoracic-belt. A comprehensive technical description of the system can be found in another publication¹¹.

2. METHODS

2.1 Software Design

2.1.1 EIT measurement simulation

A 2D high-resolution geometry of the human thorax ($\Delta x, \Delta y=1.24$ mm, ~ 50000 cells), taken from an axial MRI scan of a woman's torso⁴, was employed for simulating the expected measurements of an EIT system from a physical body. A manual segmentation was performed into eight major tissue types (figure

1), each assigned with an appropriate conductivity value for an excitation frequency of 20 kHz⁴. The heart anatomical geometry during the cardiac-cycle was extracted from time equally spaced frames of MRI², yielding a total of nineteen conductivity distribution images, starting from end-diastole, through end-systole and back to end-diastole. Figure 1 shows two examples for the thorax anatomy used for the model relating to end-systole (frame 10) and end diastole (frame 1), along with the assigned conductivity values. An eight-electrode EIT system was simulated by associating eight, equally angular-spaced boundary-cells with the surface electrodes, from which current can be injected and voltages are measured. Only opposite injections were considered for the simulations, resulting in a maximal number of 28 independent measurements ($4_{\text{injections}} \times 7_{\text{relative voltages}}$). The surface potentials were calculated by solving the governing Laplace equation with Neumann type boundary condition, valid under the quasi-static approximation for linear and isotropic media:

$$\nabla \cdot (\sigma \nabla \psi) = 0, \quad \sigma \frac{\partial \psi}{\partial \mathbf{n}} = \begin{cases} \vec{\mathbf{J}}, & \text{on electrode positions} \\ 0, & \text{elsewhere} \end{cases} \quad (1)$$

where σ [$S \cdot m^{-1}$] is the tissue conductivity, ψ [V] is the electric potential, $\vec{\mathbf{J}}$ [$A \cdot m^{-2}$] is the injected current density and \mathbf{n} is a unit vector normal to the boundary. The finite-volume method was employed for the discretization and the numerical solution of the integral presentation of the governing equation¹.

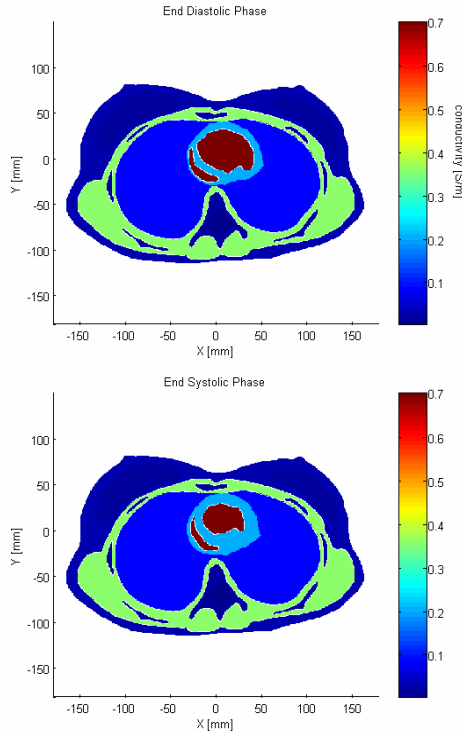


Figure 1 – end diastolic phase (top) and end systolic phase (bottom) geometrical models

2.1.2 EIT inverse problem algorithm

An iterative parametric optimization scheme, based on the Newton-Raphson method, was implemented for estimating the lengths of the major and minor axes of an elliptic-model left ventricle (LV). The geometry resolution for the inverse problem algorithm was about four times lower than that used for the forward simulations ($\Delta x, \Delta y=4.34\text{mm}$, ~ 4000 cells) for two reasons. First, it was preferred under operation time limitations as the iterative inverse problem involves many repetitions of the time-consuming forward solver. Second, geometrical discrepancies between the model for the EIT measurement simulation, i.e. the one that represents a physical measured body, and the representative model for the EIT reconstruction, were inherently included. The method comprises of guessing initial axes' lengths, appropriate for the end-systolic phase, generating a respective low-resolution conductivity distribution consisting of a proper LV size and calculating the expected surface electrode voltages. These voltages are then compared to the "real" measured, i.e., simulated, voltages using a Euclidian distance, and the axes' lengths initial guess is updated to bring that error-representing distance to a minimum. This procedure is repeated until either the error is reduced below a certain threshold or a predefined number of iterations has reached. The generation of the proper conductivity distribution map at each of the iterative stages was accomplished as follows. For the k^{th} iteration, the parameter vector update is¹⁰:

$$\mathbf{P}_{k+1} = \mathbf{P}_k - \left(\mathfrak{J}_k^T(\mathbf{P}_k) \mathfrak{J}_k(\mathbf{P}_k) \right)^{-1} \mathfrak{J}_k^T(\mathbf{P}_k) (\boldsymbol{\psi}_S(\mathbf{P}_k) - \boldsymbol{\psi}_0) \quad (2)$$

where $\mathbf{P}_k = [\mathbf{r}_{\text{minor}}, \mathbf{r}_{\text{major}}]$ is the LV axes' radii parameter vector at the k^{th} iteration, $\boldsymbol{\psi}_S(\mathbf{P}_k)$ is a concatenated vector of the surface potentials calculated for all current injections at the k^{th} iteration, $\boldsymbol{\psi}_0$ is a similar concatenated vector containing the measured surface voltages, and \mathfrak{J}_k is the k^{th} iteration

Jacobian matrix, defined as $\mathfrak{J}_k = \frac{\partial \boldsymbol{\psi}_S(\mathbf{P}_k)}{\partial \mathbf{P}_k}$. A

constant low-resolution conductivity map was obtained by decimating the original high-resolution map appropriate for the end-diastolic phase (see 2.1.1) by a ratio of 2:7. This map consisted of all the original tissues, except that the LV was omitted and replaced by a cardiac muscle tissue. For a certain iteration parameters guess, an appropriate ellipse was artificially implanted, having appropriate axes. The ellipse was centered and oriented according to the best-fit ellipse modeling the LV at end-diastole. This technique was justified by the observation that during the cardiac-cycle, the cardiac muscle contracts and expands, almost entirely on the expense of the LV domain. To avoid the geometrical discrepancies influence on the reconstructed parameters, a differential scheme was adopted. In that sense, the

"real" (simulated) measurements, ψ_0 , needed for the reconstruction algorithm, were constructed by adding the difference voltages between a certain cardiac-cycle phase and the end-systolic phase (as were simulated in 2.1.1) to a reference voltages set appropriate for an end-systolic phase, which was generated for the same geometry used as the first guess for the inverse solver. It is therefore that the algorithm is indicative only to the relative change of the LV size at a certain phase with respect to its end-systolic size.

2.2 Experimental Procedure

A preliminary study was conducted on a group of 28 subjects (all males, aged 50 ± 19 years). An inclusion criterion for subject participation in the study was inexistence of a cardiac pace maker, and all subjects signed an informed consent. The measurement procedure was carried out as follows: two bio-impedance measurements were taken using the PulmoTrace™ system (figure 2) – one measurement at end-systole (ES) and another at end-diastole (ED). These measurements were synchronized using a simultaneously measured ECG signal. To ensure minimal inter-subject variance, all measurements were taken in similar postures on a seated subject during tidal respiration, with the electrode belt attached to the patients' thorax on the plane of the fifth intercostal space in the midclavicular line using conventional ECG Ag/AgCl disposable electrodes. Eight specially designed elongation mechanisms on the electrode belt were used for adapting the electrode belt length to the thoracic perimeter of the subject, ensuring a fixed angular distance between the electrodes. In addition to the bio-impedance measurements, the SV for each subject was measured by the commercially available BioZ® (Cardiodynamics) for a reference.

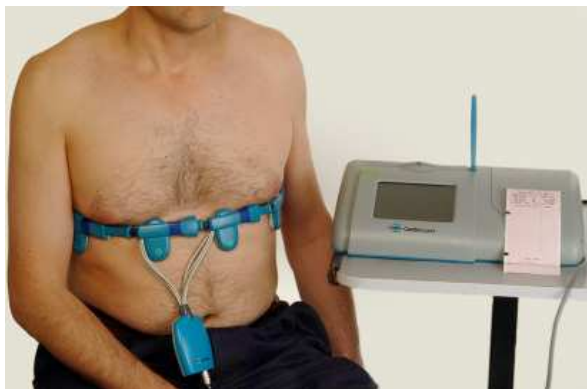


Figure 2 – PulmoTrace™ measuring system

3. RESULTS

3.1 Simulation Study

The reconstructed LV volume was compared to the "anatomical" volume along the 19 cardiac-cycle frames in figure 3(a). The volumes were calculated from the LV major and minor axes using the following relation, known as the ellipsoid-biplane model:

$$V_{LV} = \frac{8}{3\pi} \frac{(\pi r_{\min} \text{ or } r_{\max})^2}{r_{\max}} \quad (3)$$

where r_{\min} and r_{\max} are taken either directly from the anatomical images (similar to the echocardiography procedure) or from the last iteration parameter vector for the "anatomical" and reconstructed volumes, respectively. A good correlation between the true and reconstructed values can be observed ($r=0.97$, $p\text{-value}=2 \cdot 10^{-11}$). In figure 3(b), the stroke-volume error, measured as the standard deviation of $SV = V_{LV}(ED) - V_{LV}(ES)$, is plotted versus the measuring system SNR [dB], simulated by adding white Gaussian noise to the measurement leads with magnitudes between 35 and 80dB, demonstrating an exponential dependence.

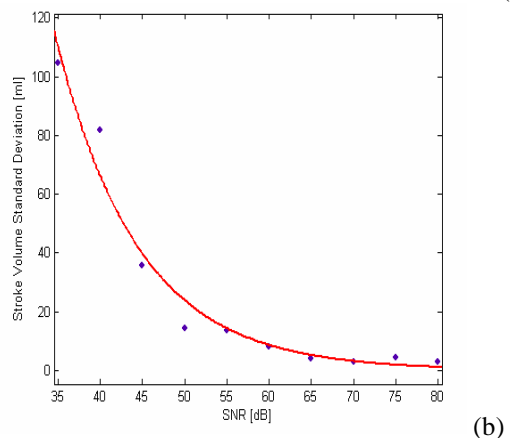
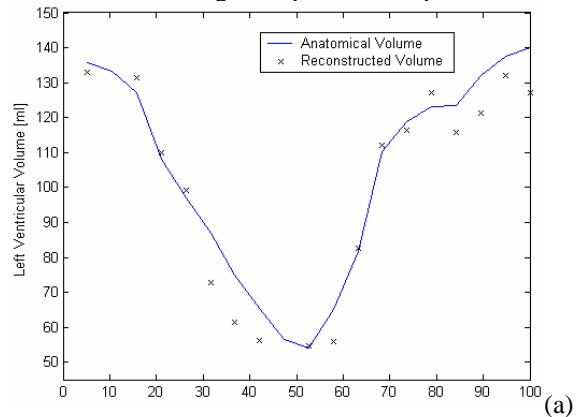


Figure 3 – a. left ventricular volume vs. cardiac cycle percentage out of anatomical (solid) and reconstructed (crosses) major and minor axes. b. SV error (dots) vs. SNR.

3.2 Clinical Study

Figure 4(a) shows the relationship between the PulmoTrace™ and the BioZ® measured stroke-volumes. A high correlation ratio of $R=0.86$ ($p\text{-value}=4\cdot 10^{-9}$) was found between the two data sets. A paired t-test showed that the two data measurement sets are not significantly separated ($p_{t\text{-test}}=0.77$). An analysis of differences was performed (Figure 4(b)), demonstrating that the two data sets are not biased (mean of difference is -1.3 ml), and that all samples but two are bounded within the $\pm 2SD$ limits. Additionally, no dependence of the difference on the mean value is apparent.

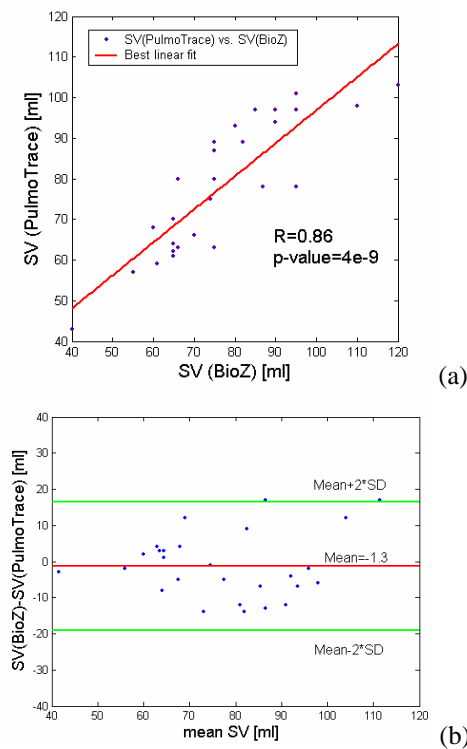


Figure 4 – a. correlation plot between $SV(\text{PulmoTrace}^{\text{TM}})$ and $SV(\text{BioZ}^{\text{®}})$. b. analysis of differences plot.

4. DISCUSSION

In this work, the feasibility of a parametric EIT algorithm for measuring stroke volume was assessed in simulation and in a clinical study. The simulations demonstrated the technique's applicability for systems with SNR values larger than ~ 60 dB (figure 3(b)), implying, in that aspect, that the PulmoTrace™ measuring system, having a measured SNR of 75dB, is appropriate. Several simplifications were adopted for this study, making the reconstruction algorithm relatively simple and fast, thus appropriate for real-time operation in clinical devices. The simulations were entirely performed for 2D settings, and should therefore be ideally extended to 3D geometry models to allow better correspondence with real, physical

obtained data. Moreover, the current model considers only the volume change of the LV during the cardiac cycle, whereas a more detailed model should also account for the blood perfusion to the peripheral organs (and consequently the conductivity alterations of these tissues), as well as the geometrical perturbations during the cardiac cycle, originating e.g. from the blood vessels dilation. Still, the clinical study showed that a good correlation exists between the stroke-volume measured using the proposed algorithm, as embedded in the PulmoTrace™ system, and the measurements of the reference BioZ® system, supporting the parametric reconstruction algorithm incentive.

5. REFERENCES

1. Abboud S, Eshel Y, Levy S, and Rosenfeld M, Numerical calculation of the potential distribution due to dipole sources in a spherical model of the head, *Comput. Biomed. Res.* 27:441-455, 1994
2. Boese JM, Bahner ML, Albers J, and Schad LR, Computed tomography of the heart with high temporal resolution using retrospective cardiac gating, From: www.dkfz-heidelberg.de/mrphys/heart/ct/ekgct.html, El-Khoury GY, Bergman RA, and Montgomery WJ, *Sectional Anatomy by MRI*. Churchill Livingstone, New-York, 1995, pp. 392
3. Gabriel C, Andreuccetti D, Fossi R, and Petrucci C, An internet resource for the calculation of the dielectric properties of body tissues, From: <http://niremf.iroec.fcnr.it/tissprop/>, 2005
4. Kubicek WG, Patterson RP, and Witsoe DA, Impedance cardiography as a non-invasive method to monitor cardiac function and other parameters of the cardiovascular system. *Ann. NY Acad. Sci.* 170:724-732, 1970
5. Moshkovitz Y, Kaluski E, Milo O, Vered Z, and Cotter G, Recent developments in cardiac output determination by bioimpedance: comparison with invasive cardiac output and potential cardiovascular applications. *Curr. Opin. Cardiol.* 19:229-237, 2004
6. Newell JC, Blue RS, Isaacson D, Saulnier GJ, and Ross AS. Phasic three-dimensional impedance imaging of cardiac activity, *Physiol. Meas.* 23(1):203-9, 2002
7. Newman DG, and Callister R, The non-invasive assessment of stroke volume and cardiac output by impedance cardiography: a review, *Aviation Space and Environ. Med.* 70(8):780-789, 1999
8. Wang L, and Patterson R, Multiple sources of the impedance cardiogram based on 3-D finite difference human thorax models, *IEEE trans. Biomed. Eng.* 42(2):141-148, 1995
9. Yorkey TJ, Webster JG, and Tompkins WJ, Comparing reconstruction algorithms for electrical impedance tomography, *IEEE Trans. Biomed. Eng.* BME-34:843-852, 1987
10. Zlochiver S, Arad M, Radai MM, Barak-Shinar D, Krief H, Engelman T, Ben-Yehuda R, Adunsky A, and Abboud S, A portable bio-impedance system for monitoring lung resistivity, *Med. Eng. & Phys.* submitted